Microstructural evolution and bonding mechanisms of the brazed Ti/ZrO_2 joint using an $Ag_{68.8}Cu_{26.7}Ti_{4.5}$ interlayer at 900 °C

Shen-Hung Wei and Chien-Cheng Lin[a)]
Department of Materials Science and Engineering, National Chiao Tung University, Hsinchu 300, Taiwan

(Received 18 November 2013; accepted 24 January 2014)

In this study, 3 mol% Y_2O_3-stabilized zirconia (3Y–ZrO_2) and commercially pure titanium (cp-Ti) joints were fabricated with an $Ag_{68.8}Cu_{26.7}Ti_{4.5}$ interlayer (Ticusil) at 900 °C for various brazing periods. After brazing at 900 °C/0.1 h, Ti_2Cu, TiCu, Ti_3Cu_4, and $TiCu_4$ layers were present at the Ti/Ticusil interface, while TiCu and TiO layers were observed at the Ticusil/3Y–ZrO_2 interface. In the residual interlayer, clumpy $TiCu_4$ was formed along with the Ag solid phase. After brazing at 900 °C/1 h, Ti_3Cu_3O and Ti_2O layers were formed at the interlayer/ZrO_2 interface, while Cu_2O was precipitated in the residual interlayer with $[111]_{Cu_2O}//[111]_{Ag}$ and $(20\bar{2})_{Cu_2O}//(20\bar{2})_{Ag}$. After brazing at 900 °C/6 h, a two-phase (α-Ti + Ti_2Cu) region was observed on the Ti side with $[2\bar{1}\bar{1}0]_{\alpha-Ti}//[100]_{Ti_2Cu}$ and $(0002)_{\alpha-Ti}//(0\bar{1}3)_{Ti_2Cu}$, while the TiCu layer grew at the expense of Ti_3Cu_4 and $TiCu_4$. The bonding mechanisms and diffusion paths were explored with the aid of Ag–Cu–Ti and Ti–Cu–O ternary phase diagrams.

I. INTRODUCTION

The Ag–Cu eutectic alloy with 28Cu (wt%) is frequently used in the conventional brazing of Ti alloys and other materials at temperatures higher than 800 °C.[1] The brazed assembly exhibits good bonding strength, resulting from the formation of Ti–Cu compounds that enhance the wettability of the solid/liquid interface.[2,3] However, Sn, Ag, Cu, Ni, Co, and Fe exhibit very poor wettability on the surface of ceramics.[4] The wettability can be significantly improved by adding active metals, such as Ti, Zr, and Hf, to the brazing filler. These metals can effectively reduce the interfacial energy by their strong chemical attraction to the oxide ceramic and can enhance the wetting behavior,[5] which even enables the surface of the ceramic to be wetted by the formation of the intermediate layer during brazing and provides a good joint.[6,7]

Hanson et al.[7] observed that a small percentage of Ti addition (~4.5Ti wt%) to the braze alloy led to a significant increase in the four-point bend strength of a PSZ–PSZ (PSZ, partially stabilized zirconia) joint. In comparison with PSZ–PSZ or PSZ-stainless steel joints, the 3Y–ZrO_2/Ti brazing couple using a Cusil ABA [63Ag–35.25Cu–1.75Ti (wt%)] had a superior joint strength due to the suitable reaction layers at the interface. The microstructural evolution at the interface between the Ti alloy (or ZrO_2) and braze alloy has been previously explored based on microstructural characterization using scanning electron microscopy (SEM)/energy dispersive spectroscopy (EDS).[1–3,6,8] However, the SEM/EDS spatial resolution was limited to the micro range (<2 μm) and unable to analyze the crystal structures. In this study, the braze filler of Ticusil [68.8Ag–26.7Cu–4.5Ti (wt%)] was selected to join the 3Y–ZrO_2 and Ti at 900 °C for various brazing periods. The objective was to elucidate the microstructural evolution and bonding mechanisms of the sandwiched Ti/Ticusil/3Y–ZrO_2 joints based on the microstructural characterization using SEM/EDS and transmission electron microscopy (TEM)/EDS.

II. EXPERIMENTAL

Hot pressed 3 mol% Y_2O_3-stabilized ZrO_2 bulks [3Y–ZrO_2, 3 mm thickness on average, with an apparent density of 5.9 g/cm^3, mainly >94ZrO_2 + HfO_2, <5.4Y_2O_3 (wt%), Toyo Soda Mfg. Co., Tokyo, Japan] and commercially pure titanium billets [cp-Ti, 5 mm thickness on average, mainly 99.31Ti–0.30Fe–0.25O (wt%), Kobe Steel, Ltd., Tokyo, Japan] were used as starting materials. The 3Y–ZrO_2 and Ti were brazed by a Ticusil interlayer [50 μm thick, 68.8Ag–26.7Cu–4.5Ti (wt%), Wesgo, Inc., Belmont, CA] under 0.1 MPa at 900 °C for 0.1, 1, and 6 h in a tube furnace (Model STF54434C, Lindberg/Blue, Thermo Elec. Inc., TX). The process temperature (900 °C) was selected to be 70 °C above the eutectic point of the filler. To prevent the sample from being oxidized, the working chamber was preevacuated to 1×10^{-4} Pa and purged with Ar (99.99% pure) to 1 atm for at least four cycles. The heating and cooling rates were 5 and 3° C/min, respectively.

Cross-sectional SEM specimens were cut, ground, and finally polished using conventional standard procedures. Then the microstructures of various reaction zones were

a)Address all correspondence to this author.
e-mail: chienlin@faculty.nctu.edu.tw
DOI: 10.1557/jmr.2014.30

 © Materials Research Society 2014

https://doi.org/10.1557/jmr.2014.30 Published online by Cambridge University Press

characterized using a SEM (Model JSM 6500F, JEOL Ltd., Tokyo, Japan) operating at 15 kV, which was equipped with an EDS (Model ISIS 300, Oxford Instrument Inc., London, U.K.). Cross-sectional TEM specimens were prepared using a focused ion beam (FIB, Model Nova 200, FEI Co., Hillsboro, OR) and the lift-out technique.[9] Typical TEM specimens had dimensions of approximately 17 μm in width and 2 μm in depth. FIB milling was performed with a Ga^+ ion beam at 30 keV. Before the FIB milling, a Pt layer approximately 1 μm thick was deposited by ion beam chemical deposition using $C_9H_{16}Pt$ as the precursor gas. The Pt layer served two main purposes: being a marker illustrating the location and protecting the sample from being directly exposed to Ga^+ ion beam implantation. After rough milling (7–1 nA), polishing (0.5–0.1 nA), and final polishing (50–10 pA), a thin foil (17 × 2 × 0.05 μm) was cut off, and then, a micromanipulator was used to transfer the foil from the sample to a TEM grid (Formvar/carbon coated-copper 200 mesh) for subsequent TEM analyses.

The interfacial microstructures of the jointed samples were then observed using an analytical TEM (Model JEM 2000 FX, JEOL Ltd, Tokyo, Japan). The Cliff–Lorimer standardless technique was performed to analyze the chemical compositions of various phases using an ultra-thin window energy dispersive spectrometer (EDS, ISIS 300, Oxford Instrument Inc., London, U.K.) attached to the TEM.[10,11] Based on the thin-film criterion, assuming that the effects of absorption and fluorescence could be neglected, all the measurements were conducted on the K_α lines of corresponding elements from the very thin regions of the TEM specimens. The standardless k factors in the Cliff–Lorimer equation had the same precision as the ones measured by the standard approach if the thin-film criterion of K_α lines was fulfilled.[11] The crystal structures and lattice parameters were determined from analysis of the selected area diffraction patterns (SADPs) using the computer-simulation software of crystallography (CaRIne Crystallography 3.1, DIVERGENT S. A., Compiègne, France).

III. RESULTS AND DISCUSSION

A. SEM/EDS analyses

Figure 1 presents a backscattering electron image (BEI) of the as-received Ticusil foil after annealing at 900 °C for 1 h. The clumpy Ag-rich phase was observed in addition to the lamellar eutectic structure of (Ag) + (Cu) within the Ticusil foil. In addition, the Ti_3Cu_4 phase [42.5Ti–56.7Cu–0.8Ag (at.%)] was also observed. It was believed that the reactions between Ti and Cu pushed the Ag–Cu composition into the hypoeutectic region, resulting in the formation of a clumpy proeutectic Ag-rich phase and the lamellar eutectic. The eutectic lamellae consisted of the bright Ag-rich phase and the dark Cu-rich phase. Furthermore, because the solubility of Cu in Ag was limited,[12] small spherical Cu-rich particles were precipitated from the Ag phase during subsequent cooling, which was consistent with the observations by Lin et al.[13]

Figure 2 presents the BEIs of the interfacial microstructure in between Ti and Ticusil (or Ticusil and 3Y–ZrO_2)

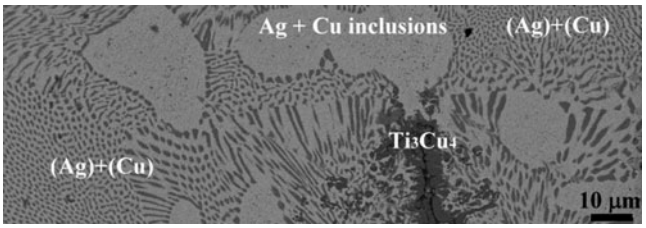


FIG. 1. SEM BEI microstructure of the as-received Ticusil foil before joining and after annealing at 900 °C for 1 h, showing the Ag–Cu eutectic, Ti_3Cu_4 phase, and Ag solid phase with Cu inclusions.

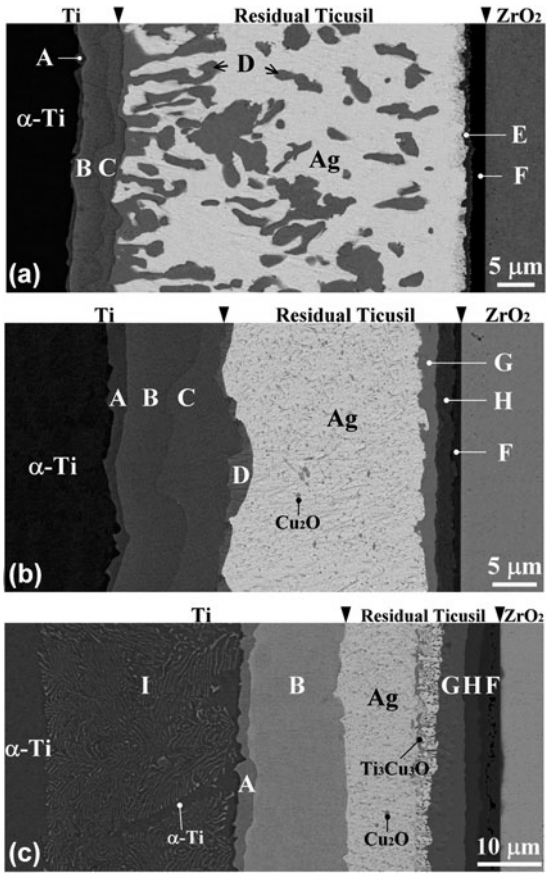


FIG. 2. SEM BEI microstructure of the Ti/Ticusil/3Y–ZrO_2 joint after brazing at 900 °C for (a) 0.1 h, (b) 1 h, and (c) 6 h, showing the reaction layers at the Ti/Ticusil interface [Ti_2Cu (A), TiCu (B), Ti_3Cu_4 (C), $TiCu_4$ (D), and α-Ti + Ti_2Cu (I)], the reaction layers at the Ticusil/3Y–ZrO_2 interface [TiCu (E), TiO (F), Ti_3Cu_3O (G), and Ti_2O (H)], and the residual Ticusil interlayer [$TiCu_4$ (D), Cu_2O, Ti_3Cu_3O, and Ag-rich phase].

https://doi.org/10.1557/jmr.2014.30 Published online by Cambridge University Press

after brazing at 900 °C for various brazing periods. The original Ti/Ticusil and Ticusil/3Y–ZrO_2 interfaces were marked by arrows. The dissolution of the Ti substrate into the liquid interlayer was thought to be much more prominent compared with that of the 3Y–ZrO_2 substrate. Figure 2(a) reveals the BEI of the Ti/Ticusil/3Y–ZrO_2 joint after brazing at 900 °C for 0.1 h. Four distinct interfacial layers (marked A, B, C, and D) existed between Ti and Ticusil. The relative contrast of the interfacial layers reflected a decreasing Ti/Cu ratio from the left to right sides because of the atomic number effect on the BEI. The thinner layer A was tentatively identified as a Ti_2Cu layer. Layer B consisted of 47.7Ti–48.6Cu–3.7Ag (at.%), indicating that layer B was TiCu. Layer C contained 41.4Ti–57.0Cu–1.6Ag (at.%) adjacent to the original interface between Ti and Ticusil, corresponding to the Ti_3Cu_4 phase. A dendritic $TiCu_4$ phase (marked D), consisting of 21.3Ti–77.2Cu–1.5Ag (at.%), tended to grow into the residual interlayer. A clumpy phase (marked D, $TiCu_4$) was observed together with the Ag solid phase within the residual interlayer. In addition, the reduction of 3Y–ZrO_2 by the Ticusil interlayer[7,14] led to the formation of a dark layer (F), consisting of 49.3Ti–48.9O–1.8Cu (at.%), which corresponds to the TiO phase. The dissolved Ti reacted with Cu to form a relatively gray layer (marked E), corresponding to the TiCu phase, near the TiO layer in the residual interlayer. The TiO layer existed as a diffusion barrier layer that limited the migration of Zr into the residual interlayer.[15] The consumption of Cu atoms due to the formation of various Ti–Cu compounds in the molten interlayer resulted in the deviation of the residual interlayer from the Ag–Cu eutectic toward the Ag-rich region.[16] Therefore, the Ag solid phase was observed throughout the residual interlayer after cooling. The Ag solid phase in the residual interlayer consisted of 94.4Ag–2.0Ti–3.6Cu (at.%) based on the EDS analyses. In this case, the yttrium (the stabilizer of ZrO_2) was not detected in TiO, indicating that the original interface was located between TiO and 3Y–ZrO_2. Figure 2(b) displays the reaction layer sequence of α-Ti/Ti_2Cu(A)/TiCu(B)/Ti_3Cu_4(C)/$TiCu_4$(D)/residual interlayer/Ti_3Cu_3O(G)/Ti_2O(H)/TiO(F)/ZrO_{2-x} in the Ti/Ticusil/3Y–ZrO_2 joint after brazing at 900 °C for 1 h. The fact that layer Ti_2Cu_3 was missing between Ti_3Cu_4 and $TiCu_4$ could be explained by kinetics considerations.[17] The residual interlayer contained the Ag solid phase, with fine Cu_2O precipitates replacing the clumpy $TiCu_4$ phase. Two oxide layers (G and H) were observed to abut the TiO layer, indicating that an extensive reduction of ZrO_2 to oxygen-deficient zirconia occurred due to the dissolved Ti in the molten interlayer. Furthermore, O exhibited a higher reactivity with Cu than Ag such that the Cu_2O phase was formed in the Ag solid phase during cooling. According to the Ti–Cu–O ternary phase diagram,[18] the Ti–Cu–O compound would be formed while exceeding the maximum solubility of O (~2 at.%) in the TiCu. For comparison, the reaction zone between the Ag–Cu–Sn–Ti filler metal and Al_2O_3 was comprised of two sublayers after brazing at 900 °C for 20 min: an fcc γ-TiO layer and another sublayer of Ti_3Cu_3O with a diamond cubic structure, which provided a more reliable joint than TiO alone.[19] Figure 2(c) illustrates the reaction layer sequence of α-Ti/α-Ti + Ti_2Cu(I)/Ti_2Cu(A)/TiCu(B)/residual interlayer/Ti_3Cu_3O(G)/Ti_2O(H)/TiO(F)/ZrO_{2-x} in the sandwiched joint after brazing at 900 °C for 6 h, where the Cu_2O, Ti_3Cu_3O, and Ag phases were present in the residual interlayer. Cu diffusion from the interlayer to the Ti substrate led to the hypoeutectoid transformation of a two-phase layer (α-Ti + Ti_2Cu), designated as I, during a long-term brazing period.[20] The elongated α phase in the (α-Ti + Ti_2Cu) region corresponded to a proeutectoid phase. The transformation could be written by two steps of the hypoeutectoid reaction: β-Ti → β_1-Ti + α-Ti (proeutectoid α-Ti) and β_1-Ti → Ti_2Cu + α-Ti (eutectoid α-Ti). The formation Gibbs free energies (ΔG^0) of Ti_2Cu and TiCu were more negative than those of Ti_3Cu_4 and $TiCu_4$.[21] Therefore, it was believed that a further reaction could occur between Ti_3Cu_4 (or $TiCu_4$) and Ti to produce the more stable TiCu phase.

B. TEM/EDS analyses

1. Microstructure at the Ticusil/3Y–ZrO_2 interface

Figure 3(a) presents a bright field image (BFI) of two suboxide layers, corresponding to TiO and Ti_2O (labeled F and H) in the Ti/Ticusil/3Y–ZrO_2 joint after brazing at 900 °C/1 h. Figures 3(b) and 3(c) display the SADPs of the β-TiO with the incident electron beam along the zone axes of [001] and [111], respectively, indicating that the material had a cubic structure similar to the NaCl structure, with the measured lattice parameter a = 0.4234 nm (β-TiO, *Fm3m*, a = 0.4185 nm in JCPDS No. 772170).[22] Note that the reflections should be absent due to the zero structure factor for such planes as $(0\bar{1}0)$, (100), $(10\bar{1})$, and $(1\bar{1}0)$ but appeared in the pattern due to double diffraction and the nonstoichiometric composition. Figures 3(d) and 3(e) present the SADPs of Ti_2O on the zone axes of $[\bar{1}2\bar{1}0]$ and $[\bar{2}4\bar{2}\bar{3}]$, respectively, identified as a hexagonal structure with the measured lattice parameters a = 0.2898 nm and c = 0.48765 nm (Ti_2O, $P\bar{3}m1$, a = 0.2953 nm, c = 0.48454 nm in JCPDS No. 731582).[23] Figure 3(f) demonstrates that the β-TiO consisted of 49.65Ti–47.33O–1.76Zr–1.26Cu (at.%). Figure 3(g) presents the EDS results of Ti_2O, indicating that the material consisted of 65.46Ti–30.3O–3.12Zr–1.12Cu (at.%).

ZrO_2 tends to be reduced to an oxygen-deficient zirconia (ZrO_{2-x}) in a reducing environment.[24] Because Ti has a high affinity for O, it can act as a reducing agent of ZrO_2. When Ti is in contact with ZrO_2, oxygen can diffuse out of ZrO_2 and be dissolved in Ti, leading to the formation of ZrO_{2-x}, even though the Ellingham diagram

https://doi.org/10.1557/jmr.2014.30 Published online by Cambridge University Press

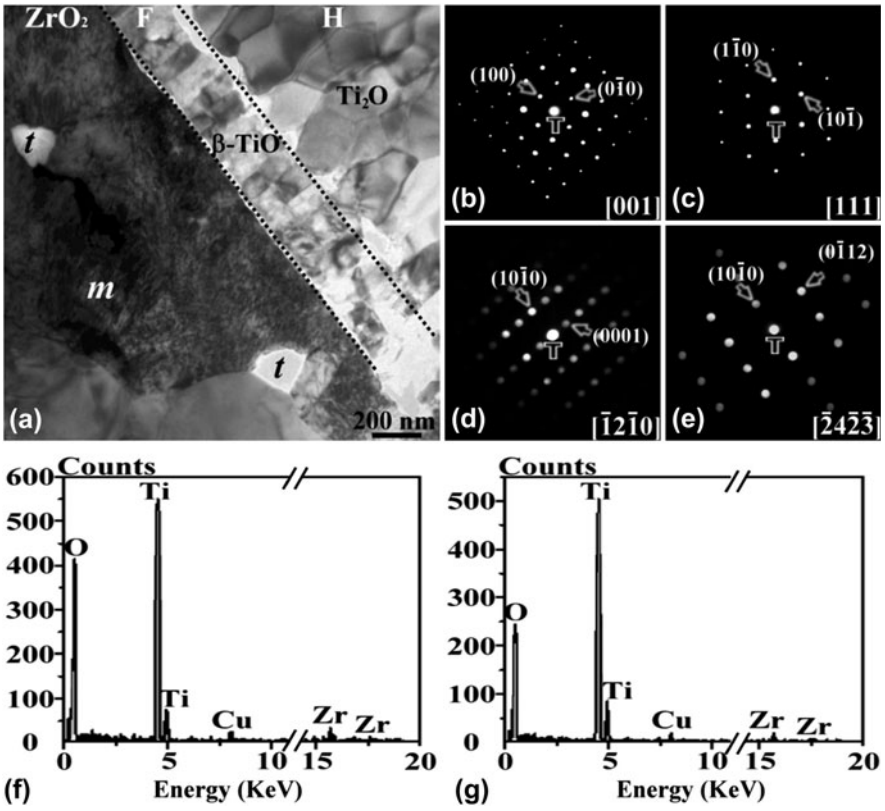


FIG. 3. TEM results of the microstructure: (a) morphology of β-TiO and Ti_2O at the Ticusil/3Y–ZrO_2 interface of the Ti/Ticusil/3Y–ZrO_2 joint after brazing at 900 °C for 1 h; (b and c) electron diffraction patterns of β-TiO with the [001] and [111] zone axes, respectively; (d and e) electron diffraction patterns of Ti_2O with the $[\bar{1}2\bar{1}0]$ and $[\bar{2}4\bar{2}\bar{3}]$ zone axes, respectively; (f) EDS spectrum of β-TiO; and (g) EDS spectrum of Ti_2O.

indicates that ZrO_2 is more thermodynamically stable than TiO_2. Thus, ZrO_2 is not completely reduced into the metallic Zr, while Ti is not oxidized as TiO_2 in the partial reduction and dissolution process mentioned above. However, certain titanium oxides are likely formed as the amount of dissolved oxygen increases in Ti. In this study, ZrO_2 was partially reduced by Ti to become ZrO_{2-x}, while oxygen was dissolved into the residual interlayer to form the intermediate compounds TiO, Ti_2O, and Ti_3Cu_3O. The liquid Ticusil exhibited good wettability on the 3Y–ZrO_2 surface due to the formation of TiO (metallic characteristics).[25]

2. Microstructure at the residual Ticusil interlayer

Figure 4(a) presents a BFI of the Cu_2O precipitate in the Ag-rich matrix within the residual interlayer after brazing at 900 °C for 1 h. The Ag-rich matrix was accompanied by dislocations because of the CTE (coefficient of thermal expansion) mismatch between Ticusil and 3Y–ZrO_2. Figure 4(b) displays the SADPs of the Cu_2O and Ag-rich phase with its schematic diagram redrawn in Fig. 4(c). From their superimposed SADPs, the orientation relations of Cu_2O and Ag were identified as follows: $[111]_{Cu_2O}//[111]_{Ag}$ and $(20\bar{2})_{Cu_2O}//(20\bar{2})_{Ag}$. The lattice

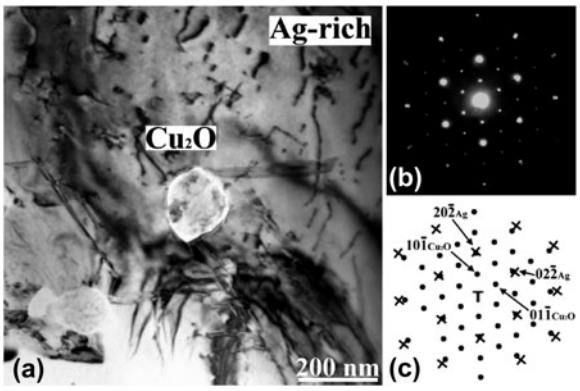


FIG. 4. TEM results of the microstructure: (a) morphology of the Cu_2O precipitates in the Ag-rich matrix of the residual Ticusil interlayer after brazing at 900 °C for 1 h and (b and c) electron diffraction patterns of Cu_2O and Ag with their schematic diagram (●, Cu_2O and ×, Ag) showing $z = [111]_{Cu_2O}//[111]_{Ag}$ and $(20\bar{2})_{Cu_2O}//(20\bar{2})_{Ag}$.

parameter of Cu_2O was measured to be 0.4264 nm (Cu_2O, *Pn3m*, a = 0.4267 nm in JCPDS No. 782076). Furthermore, the lattice parameter of fcc Ag was measured to be 0.4198 nm (Ag, *Fm3m*, a = 0.4086 nm in JCPDS No. 040783). The orientation relationship between these two phases was cube-on-cube. Because Cu_2O is an antifluorite derivative with 4 Cu atoms at 0, 0, 0 + face-centering

https://doi.org/10.1557/jmr.2014.30 Published online by Cambridge University Press

translations and 2 O atoms at 1/4, 1/4, 1/4 + body-centering translations,[26] the (*hkl*) reflection spots were absent for two even and one odd integer.

3. Microstructure at the cp-Ti/Ticusil interlayer

Figures 5(a) and 5(b) display BFIs of the Ti/Ticusil interfacial microstructure after brazing at 900 °C/1 h, revealing several phases, such as α-Ti, Ti_2Cu, TiCu, $TiCu_4$, and the Ag-rich matrix. Figure 5(c) shows the SADP of Ti_2Cu along the zone axis of [010], corresponding to a tetragonal structure with the measured lattice parameters a = 0.2941 nm and c = 1.0779 nm (Ti_2Cu, *I4/mmm*, a = 0.29438 nm, c = 1.07861 nm in JCPDS No. 720441). Figure 5(d) presents the SADP of TiCu along the zone axis of $[0\bar{2}1]$, identified as a tetragonal structure with the measured lattice parameters a = 0.323 nm and c = 0.6132 nm (TiCu, *P4/mmm*, a = 0.3108 nm, c = 0.5887 nm in JCPDS No. 070114). Figure 5(e) presents the EDS results of Ti_2Cu, consisting of 67.62Ti–31.25Cu–1.13Ag (at.%). Figure 5(f) presents the EDS results of TiCu, which consisted of 48.13Ti–47.59Cu–4.28Ag (at.%). Figure 5(g) shows that the $TiCu_4$ contained 20.05Ti–78.60Cu–1.35Ag (at.%).

Figure 6(a) demonstrates that acicular Ti_2Cu was precipitated on the titanium side of the Ti/Ticusil/3Y–ZrO_2 joint after brazing at 900 °C/6 h. Figure 6(b) displays the SADPs, with their patterns redrawn in Fig. 6(c), of α-Ti and Ti_2Cu with the following orientation relationship: $[2\bar{1}\bar{1}0]_{\alpha-Ti}//[100]_{Ti_2Cu}$ and $(0002)_{\alpha-Ti}//(0\bar{1}3)_{Ti_2Cu}$. The Ti_2Cu had a tetragonal structure with the measured lattice parameters a = 0.297 nm and c = 1.071 nm (Ti_2Cu, *I4/mmm*, a = 0.29438 nm, c = 1.07861 nm in JCPDS No. 720441), while the matrix was identified as α-Ti with the measured lattice parameters a = 0.299 nm and c = 0.474 nm (α-Ti, *P6₃/mmc*, a = 0.295 nm, c = 0.4682 nm in JCPDS No. 441294).

C. Microstructure development and diffusion path

1. Diffusion path for the Ag–Cu–Ti phase diagram

Figure 7(a) presents an isothermal section of the Ag–Cu–Ti ternary phase diagram at 900 °C.[27] The diffusion path (solid line), indicative of the compositions along the

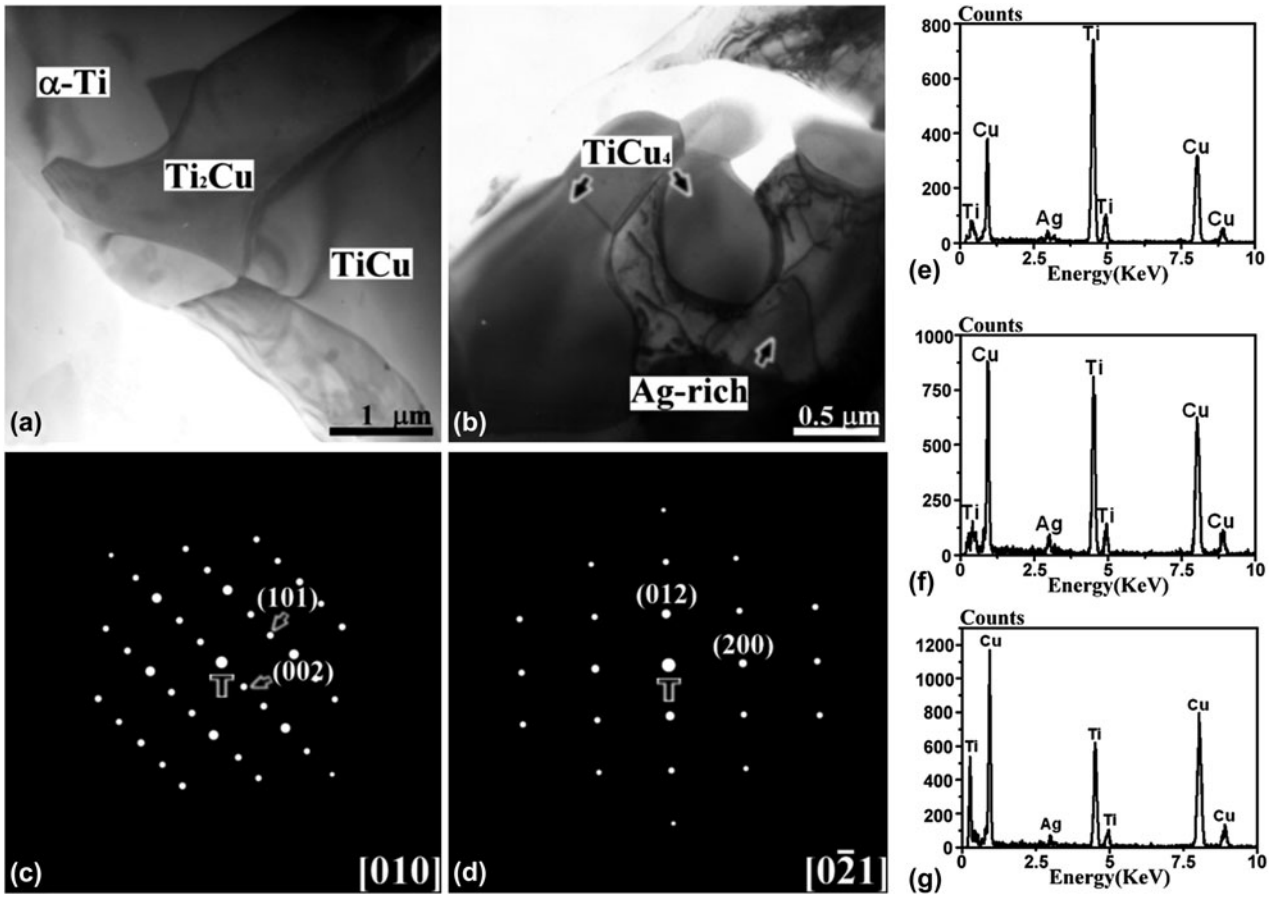


FIG. 5. TEM results of the microstructure: (a and b) morphologies of the α-Ti, Ti_2Cu, TiCu, $TiCu_4$, and Ag-rich phases at the Ti/Ticusil interface of the Ti/Ticusil/3Y–ZrO_2 joint after brazing at 900 °C for 1 h; (c) electron diffraction patterns of Ti_2Cu with the [010] zone axis; (d) electron diffraction patterns of TiCu with the $[0\bar{2}1]$ zone axis; (e) EDS spectrum of Ti_2Cu; (f) EDS spectrum of TiCu; and (g) EDS spectrum of $TiCu_4$.

https://doi.org/10.1557/jmr.2014.30 Published online by Cambridge University Press

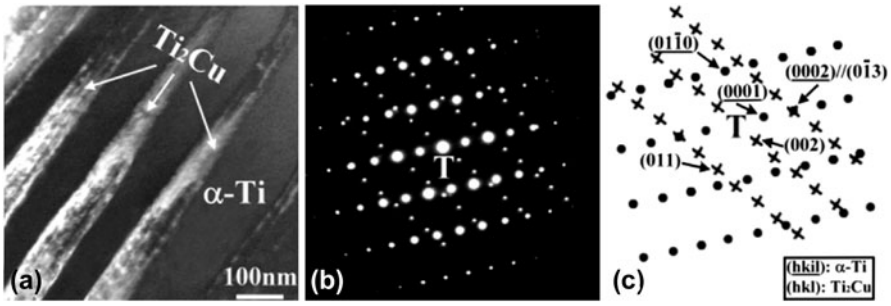


FIG. 6. TEM results of the microstructure: (a) morphology of acicular Ti_2Cu precipitates in the α-Ti matrix on the Ti side of the Ti/Ticusil/3Y–ZrO_2 joint after brazing at 900 °C for 6 h and (b and c) electron diffraction patterns of α-Ti and Ti_2Cu with their schematic diagram (●, α-Ti and ×, Ti_2Cu) showing $z = [2\bar{1}\bar{1}0]_{\alpha-Ti}//[100]_{Ti_2Cu}$ and $(0002)_{\alpha-Ti}//(0\bar{1}3)_{Ti_2Cu}$.

longitudinal direction perpendicular to the interface, was proposed to be *a–b–c–d–e–f–g–h–i–j* for the Ti/Ticusil interface after brazing at 900 °C/0.1 h. The diffusion path crossed the fields of α-Ti, α-Ti + Ti_2Cu, Ti_2Cu, Ti_2Cu + TiCu, TiCu, TiCu + Ti_3Cu_4, Ti_3Cu_4, Ti_3Cu_4 + L, and L. The diffusion path did not pass through Ti_2Cu_3 from the viewpoint of kinetics.[17] The three-phase regions and crossing parallel tie lines (not shown) in the two-phase regions of the ternary phase diagram were simply in correspondence to the layer interface. Figure 7(b) presents the microstructures that developed in the Ti/Ticusil joint upon brazing at 900 °C/0.1 h. The connecting letters indicate the relationship between the microstructure of the Ti/Ticusil interface and the isothermal section of the Ag–Cu–Ti phase diagram. As illustrated in Fig. 7(b), the regions of α-Ti + Ti_2Cu (*b* to *c*), Ti_2Cu + TiCu (*d* to *e*), TiCu + Ti_3Cu_4 (*f* to *g*), and Ti_3Cu_4 + L (*h* to *i*) correspond to the interfaces between α-Ti and Ti_2Cu, Ti_2Cu and TiCu, TiCu and Ti_3Cu_4, and Ti_3Cu_4 and L, respectively. Thus, the layers of α-Ti, Ti_2Cu, TiCu, Ti_3Cu_4, and L (Ag (major) + $TiCu_4$ (minor)) were formed in sequence from Ti to Ticusil upon cooling.

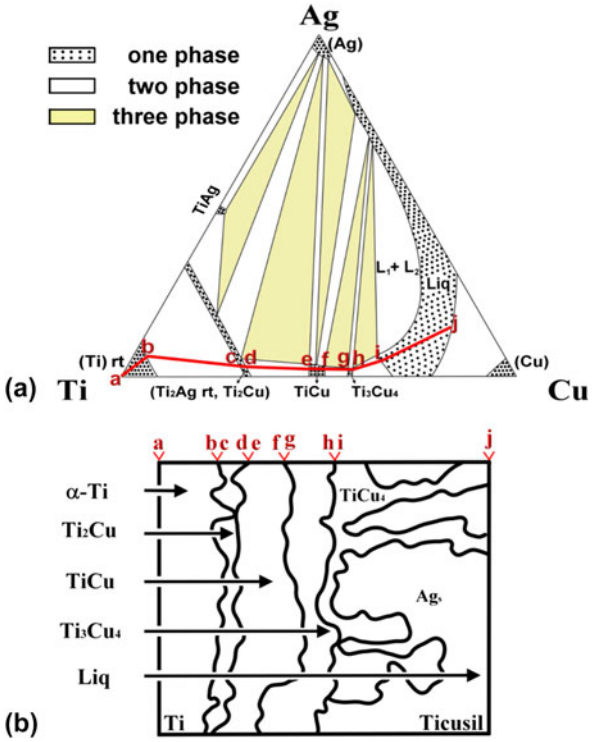


FIG. 7. (a) An isothermal section of the Ag–Cu–Ti system at 900 °C and the schematic diffusion path: *a–b–c–d–e–f–g–h–i–j* and (b) the correlation between the ternary phase diagram and the microstructural evolution at the Ti/Ticusil interface of the Ti/Ticusil/3Y–ZrO_2 joint after brazing at 900 °C for 0.1 h. L_1 and L_2 are represented as an Ag–Cu rich liquid and a Ti–Cu rich liquid, respectively.

2. Diffusion path for the Ag–Cu–Ti phase diagram

Figure 8(a) illustrates the correlation between the microstructure of the Ticusil/3Y–ZrO_2 interface and the Ti–Cu–O ternary phase diagram.[18] The diffusion path lying upon the solid line was designated as follows: *a′–b′–c′–d′–e′–f′*. The crossed fields were TiO, TiO + Ti_2O, Ti_2O, Ti_2O + Ti_3Cu_3O, and Ti_3Cu_3O. The interfaces of various reaction layers were illustrated by these regions, such as TiO + Ti_2O (*b′* to *c′*) and Ti_2O + Ti_3Cu_3O (*d′* to *e′*). The reaction layers of TiO, Ti_2O, and Ti_3Cu_3O, as illustrated in Fig. 8(b), were formed between Ticusil and 3Y–ZrO_2 after brazing at 900 °C/1 h. No Ti_3O_2 phase appeared because the peritectoid reaction (α-Ti + α-TiO → Ti_3O_2) occurred at 920 °C.

D. Proposed model of microstructural evolution

1. Melting and solidification of Ticusil

Figure 9 shows the liquidus surface projection of the ternary Ag–Cu–Ti diagram (middle)[28] and the relevant binary phase diagrams (Ti–Cu, Ag–Cu, and Ag–Ti).[12,29,30] While there are two intermetallics (Ti_2Ag and TiAg) in the Ag–Ti phase diagram,[29] six intermetallics (Ti_2Cu, TiCu, Ti_3Cu_4, Ti_2Cu_3, $TiCu_2$, and $TiCu_4$) exist in the Ti–Cu phase diagram[30] due to the high negative values for the heat of mixing. Thus, Ti has a greater affinity for Cu than for Ag. The Ticusil alloy has a composition of 55.4Ag–36.5Cu–8.1Ti (at.%), which might be considered as a eutectic $Ag_{60}Cu_{40}$ modified with 8.1Ti (at.%). Its composition (labeled M) fell inside a wide miscibility loop in the ternary Ag–Cu–Ti liquidus projection. Two arrows

https://doi.org/10.1557/jmr.2014.30 Published online by Cambridge University Press

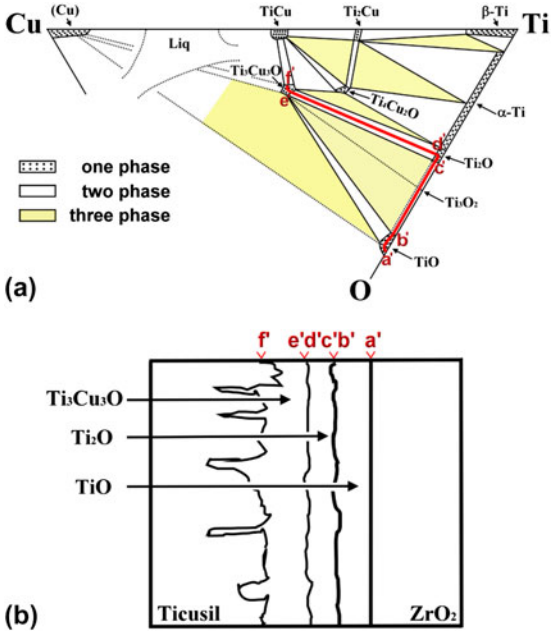


FIG. 8. (a) An isothermal section of the Ti–Cu–O system at 945 °C and the schematic diffusion path: *a′–b′–c′–d′–e′–f′* and (b) the correlation between the diffusion path and the ternary phase diagram showing the microstructural evolution at the Ticusil/3Y–ZrO_2 interface of the Ti/Ticusil/3Y–ZrO_2 joint after brazing at 900 °C for 1 h.

pointed to the compositions of L_a and L_b upon reaching the miscibility boundary line, indicating that the Ticusil was divided into two immiscible liquids: M → L_a + L_b at 900 °C. Estimated from the miscibility loop, the liquid Ticusil was separated into 20% L_a [7.1Ag–59.3Cu–33.6Ti (at.%)] and 80% L_b [67.7Ag–31Cu–1.3Ti (at.%)]. L_a was approximate to the apparent ratio Ti:Cu = 1:2, while the chemistry of L_b was close to the Ag–Cu eutectic composition [60Ag–40Cu (at.%)] at 780 °C.

Although the concentrations of Ti were quite different in both the Cu–Ti rich (L_a) and Ag–Cu rich (L_b) liquids at 33.6 and 1.3 (at.%), respectively, the two separated liquids had the same activities of Ti and Cu, respectively. Thus, Ag could enhance the activity of Ti, while Cu suppressed the activity of Ti in the liquid.[31] Because Ticusil was regarded as a modified eutectic 60Ag–40Cu (at.%) with a low content of Ti, a vertical Cu–Ti section of the Ag–Cu–Ti system [fixed 60Ag (at.%)] would be useful to analyze the solidification of the interlayer.[27]

The compositions of these two separated liquid phases were fixed with a small variation in their relative amounts as the point M was projected to the point X, in which the composition X was located at 60Ag–35Cu–5Ti (at.%). Figure 10(a) indicates that the cooling path of the point X would pass through several domains upon cooling from 900 °C as follows: (i) L_a + L_b (two liquid phases separated at 900 °C); (ii) L_a + L_b + Ti_3Cu_4 (L_a exhausted and transformed into Ti_3Cu_4 with all the Ag (L_a) and excess Cu (L_a) diffusing from L_a to L_b at 889–879 °C); (iii) L + Ti_3Cu_4 (L_b transformed into L at 879–854 °C); (iv) L + (Ag) + Ti_3Cu_4 (a solid Ag phase precipitated from L at 854–843 °C); (v) L + Ti_2Cu_3 + (Ag) (all the Ti_3Cu_4 transformed into Ti_2Cu_3 and more Ag precipitated at 843–808 °C); (vi) L + (Ag) + $TiCu_4$ (all the Ti_2Cu_3 transformed into $TiCu_4$, and more Ag precipitated at 808–783 °C); and (vii) (Ag) + (Cu) + $TiCu_4$ (L consumed completely and transformed into Ag and Cu below 783 °C). If this description was true, the final microstructures of the Ticusil interlayer should have consisted of Ag and Cu solid solutions and $TiCu_4$ precipitates. However, primary Ag with Cu inclusions, eutectic (Ag) + (Cu), and Ti_3Cu_4 were observed in the as-received Ticusil interlayer. The vertical Cu–Ti sections of the Ag–Cu–Ti system for fixed 55.4 and 60 at.% Ag were significantly different such that the relevant cooling path should be somewhere between M and X. Therefore, the cooling path could first enter the (L + TiCu + Ti_3Cu_4) domain, resulting in the isothermal reaction at 900 °C in the Ag–Cu–Ti triangle, as illustrated in Fig. 9: $L_1'' + TiCu \leftrightarrow L_2'' + Ti_3Cu_4$ (L_1'' and L_2'' were close to L_a and L_b, respectively).[28] Thus, not only two separated liquids (L_a + L_b) but also two Ti–Cu phases (TiCu + Ti_3Cu_4) existed at 900 °C. In brief, the amount of L_a was consumed with the decreasing temperature, and the remaining L_b (designated L hereafter) would follow the cooling paths from U_4 toward U_5, as shown in Fig. 10(b), in the temperature range from 900 to 843 °C as follows[17]: $U_4 : L + TiCu \rightarrow Ag + Ti_3Cu_4$ and $U_5 : L + Ti_3Cu_4 \rightarrow Ag + Ti_2Cu_3$. The solidus point of Ticusil (830 °C) corresponded to the transformation of Ti_3Cu_4 to Ti_2Cu_3. The solidification of the liquid phase would be completed at U_5. The Ti_3Cu_4 phase was retained at room temperature after cooling from 900 °C because the formation of Ti_2Cu_3 had very slow kinetics.[17] Thus, most of the Ti in the as-received Ticusil interlayer was associated with the Cu-rich phase (Ti_3Cu_4) at 900 °C.

2. Microstructural evolutions at the Ti/Ticusil/3Y–ZrO_2 interface

The model of melting and solidification mentioned above could not be applied to brazing because the reactive wetting and interdiffusion between the Ticusil interlayer melt and base materials caused the formation of Ti–Cu compounds and a dramatic compositional variation in the liquid interlayer. Based on the activity distributions of Ti and Cu, the microstructural development and bonding mechanisms of the Ti/Ticusil/3Y–ZrO_2 joint were described as follows.

In stage 1, the Ticusil interlayer was melted at 900 °C, resulting in the phase separation of L_a [7.1Ag–59.3Cu–33.6Ti (at.%)] and L_b [67.7Ag–31Cu–1.3Ti (at.%)]. These

https://doi.org/10.1557/jmr.2014.30 Published online by Cambridge University Press

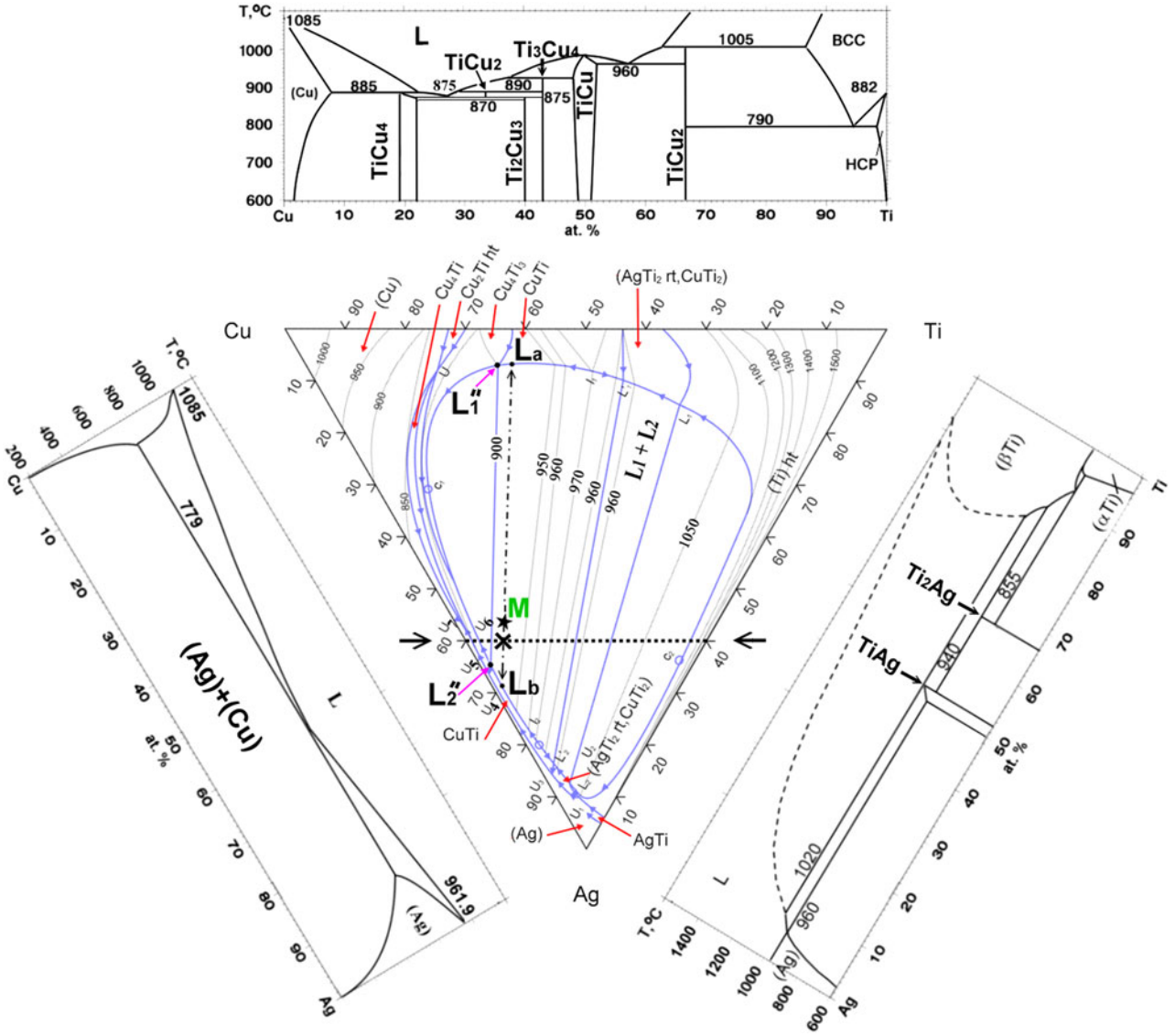


FIG. 9. Liquidus surface projection onto the Ag–Cu–Ti compositional triangle (middle), Ti–Cu binary phase diagram (top), Ag–Cu phase diagram (left), and Ag–Ti phase diagram (right). Designations: – (boundary of miscibility loop); →. . .← [vertical Cu–Ti–(60% Ag)]; ←★→ (composition of Ticusil and liquid phase separation path); M, nominal composition of Ticusil ($Ag_{55.4}$–$Cu_{36.5}$–$Ti_{8.1}$); and ×, composition of Ag_{60}–Cu_{35}–Ti_5.

two phases were in equilibrium such that the activities of the Ti and Cu in them were fixed, respectively, through the interlayer, as shown in Fig. 11(a). Because the Ti–Cu affinity was stronger than the Ag–Ti affinity, the near Ti:Cu = 1:2 stoichiometry liquid (L_a) tended to approach the Ti side, while the near Ag–Cu eutectic liquid (L_b) moved to the 3Y–ZrO_2 side. In stage 2, the Ticusil melt had a good wettability on the Ti surface because Ti was a very active metal. Good wettability could enhance the dissolution and reaction of Ti and 3Y–ZrO_2 into the Ticusil liquid. After the Ti substrate was significantly dissolved in the Ticusil interlayer, the Ti activity increased, and a gradient was established between the Ti and 3Y–ZrO_2. When the Ti activity was sufficiently high in the liquid (L_a) adjacent to the Ti surface, Ti_3Cu_4 began to nucleate and grow as a thin outer layer on the Ti surface. Once Ti_3Cu_4 was formed, the concentration of Cu adjacent to the Ti substrate was reduced, leading to a Cu activity gradient in the liquid phase abutting the Ti, as shown in Fig. 11(b). In stage 3, the predominant mechanisms were interdiffusion and a chemical reaction between Ti and the Ticusil melt. It was believed that Cu diffused across the Ti_3Cu_4 layer and reacted with Ti to produce TiCu and Ti_2Cu at the Ti/Ti_3Cu_4 interface because the Cu atoms diffused faster than the Ti atoms. Figure 11(c) shows that the activities of Ti and Cu descended in opposite directions through the three Ti–Cu layers. As the Ti–Cu layers increased in thickness, the increasing distance over which

https://doi.org/10.1557/jmr.2014.30 Published online by Cambridge University Press

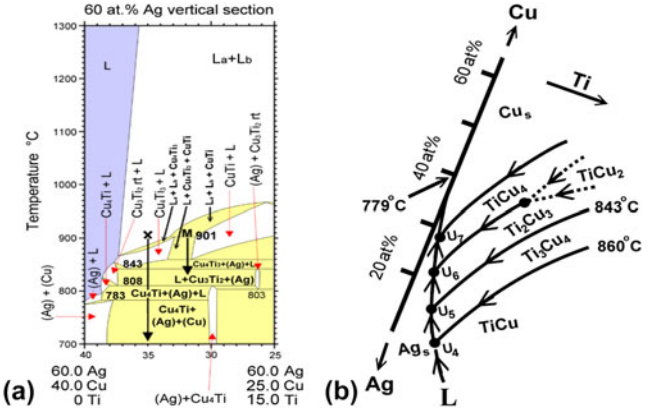


FIG. 10. (a) A vertical Cu–Ti–(60% Ag) section of the Ag–Cu–Ti system between 700 and 1300 °C and (b) the cooling paths (U_4–U_7) in the partial liquidus projection of the Ag–Cu–Ti phase diagram between 779 and 860 °C. Different colors are used for the one-phase region (purple), two-phase region (white), and three-phase region (yellow).

the Cu and Ti needed to diffuse hindered the transportation of Ti through the Ti–Cu layers. Thus, the further supply of Ti atoms to the interface was frequently negligible and insufficient, resulting in a Ti-depleted zone in liquid L_a abutting the Ti substrate after the nucleation of $TiCu_4$ occurred at the solid/liquid interface with a reduced relative Ti/Cu ratio (3/4 → 1/4). This result indicated that Ti was sharply consumed and that concentration inversion occurred. In stage 4, all the Ti in the liquid L_a was nearly consumed. Meanwhile, the $TiCu_4$ tended to grow into the liquid with more concentrated Ti and Cu (L_b) such that dendritic $TiCu_4$ would nucleate and grow into the liquid phase. The clumpy $TiCu_4$ was also formed far away from the original Ti/Ticusil interface before the complete solidification of the interlayer. The residual interlayer hereafter could be considered an Ag–Cu binary alloy (L) with a small amount of Ti in solution. However, the Cu content in the L was gradually reduced due to the formation of Cu–Ti intermetallic compounds as the composition of the liquid phase varied along the liquidus. Thus, the melting temperature would be increased somewhere in the Ag–Cu binary phase diagram.[12] It was believed that the composition of the residual Ag–Cu alloy (L) should be below the hypoeutectic limit (14 at.%) because no eutectic (Ag) + (Cu) structure was observed after cooling. Furthermore, the liquidus temperature should have been increased above 900 °C such that its composition and temperature (marked as ★) were located in the (L + Ag) region, as shown in Fig. 11(i). It was inferred that the clumpy $TiCu_4$ was formed together with the Ag solid solution in the residual interlayer after cooling from 900 °C. As Ti was dissolved in the Ticusil melt, the Ti activity in the vicinity of the 3Y–ZrO_2 interface also increased beyond a threshold value such that a thinner layer of TiO was formed at 900 °C. The near Ag–Cu eutectic liquid (L_b) spread on the 3Y–ZrO_2 substrate by reactive wetting: $xTi_{diss} + ZrO_2 \rightarrow xTiO + ZrO_{2-x}$, as shown in Fig. 11(b). Then, Cu atoms in the Ag–Cu liquid (L) reacted with Ti_{diss} to form a thinner layer of TiCu over the TiO layer, as observed in Fig. 11(c). Figure 11(d) demonstrates that the interfacial layer sequence of Ti_2Cu/TiCu/Ti_3Cu_4/residual interlayer (Ag + $TiCu_4$)/TiCu/TiO existed after brazing at 900 °C/0.1 h.

Figure 11(e) demonstrates that four continuous and thicker Ti–Cu layers (Ti_2Cu/TiCu/Ti_3Cu_4/$TiCu_4$) were formed sequentially from the Ti side to the interlayer upon brazing at 900 °C/1 h, which means that dramatic Cu consumption would cause complete solidification with the composition of the residual Ag–Cu alloy (L) being located in the α-Ag solid solution of the Ag–Cu phase diagram (marked by ▲).[12] Neither the clumpy $TiCu_4$ nor the dendritic $TiCu_4$ was observed because no liquid phase remained at this stage. After cooling, supersaturated Cu and O were precipitated as Cu_2O in the matrix of Ag. In addition to the TiO layer, two oxide layers of Ti_2O and Ti_3Cu_3O were observed on the 3Y–ZrO_2 side, which indicated that significant O atoms (from the ZrO_{2-x}) diffused across the TiO layer to react with the Cu and Ti atoms of the residual interlayer such that the residual interlayer should be considered an Ag alloy with Ti, Cu, and O in solid solutions. The formation of Ti_3Cu_3O could be described by the following reaction: $3TiCu + O_{diss} \rightarrow Ti_3Cu_3O$. Thermodynamic calculations of the Gibbs free energy (ΔG) for Ti_3Cu_3O (−502.5 kJ/mol) confirmed that it was more stable than TiCu (−14.7 kJ/mol) at 900 °C.[21,32] Finally, the interfacial layers [Ti_2Cu/TiCu/Ti_3Cu_4/$TiCu_4$/residual interlayer (Ag + Cu_2O)/Ti_3Cu_3O/Ti_2O/TiO] were observed after brazing at 900 °C/1 h, as shown in Fig. 11(f).

Figure 11(g) shows the microstructure expected before cooling for brazing at 900 °C/6 h. The TiCu phase grew at the expense of Ti_3Cu_4 and $TiCu_4$ at the Ti/Ticusil interface, indicating that TiCu was much more stable than both Ti_3Cu_4 and $TiCu_4$.[21,33] While three interfacial oxide layers (Ti_3Cu_3O, Ti_2O, and TiO) became thicker, no new phase was formed in the vicinity of the 3Y–ZrO_2. However, a two-phase region of α-Ti + Ti_2Cu appeared on the Ti side due to a hypoeutectoid reaction during cooling, implying that the extensive diffusion of Cu occurred on the Ti side. The composition of the residual interlayer went further into the (Ag) region and was located at the position marked by a dot (●) in the Ag–Cu phase diagram in Fig. 11(i). Fine Cu_2O and Ti_3Cu_3O phases were precipitated in the Ag solid solution of the residual interlayer during cooling. Finally, the interfacial layers of α-Ti + Ti_2Cu/Ti_2Cu/TiCu/residual interlayer (Ag + Cu_2O + Ti_3Cu_3O)/Ti_3Cu_3O/Ti_2O/TiO in sequence were observed after brazing at 900 °C/6 h, as shown in Fig. 11(h).

https://doi.org/10.1557/jmr.2014.30 Published online by Cambridge University Press

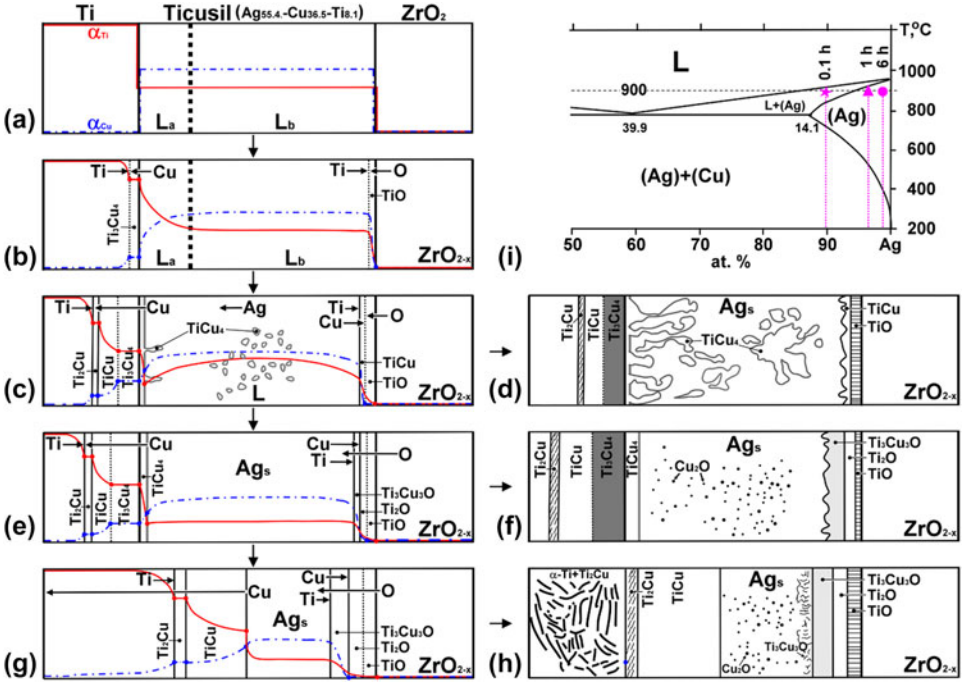


FIG. 11. Microstructural evolution of the Ti/Ticusil/3Y–ZrO_2 joint at 900 °C for various brazing periods: (a) → (b) → (c) → (d) for 0.1 h, (a) → (b) → (e) → (f) for 1 h, and (a) → (b) → (g) → (h) for 6 h. The activity profiles of Ti and Cu are depicted on an arbitrary scale for simplicity. (i) the Ag-Cu phase diagram showing the corresponding compositions for various brazing periods.

IV. CONCLUSIONS

In this study, 3 mol% Y_2O_3-stabilized zirconia (3Y–ZrO_2) and commercially pure titanium (cp-Ti) joints were fabricated with an $Ag_{68.8}Cu_{26.7}Ti_{4.5}$ interlayer at 900 °C for various brazing periods. After brazing at 900 °C/0.1 h, Ti_2Cu, TiCu, Ti_3Cu_4, and $TiCu_4$ layers were present at the Ti/Ticusil interface, while TiCu and TiO layers were observed at the Ticusil/3Y–ZrO_2 interface. After brazing at 900 °C/1 h, Ti_3Cu_3O and Ti_2O layers were formed at the interlayer/ZrO_2 interface. After brazing at 900 °C/6 h, the TiCu layer grew at the expense of Ti_3Cu_4 and $TiCu_4$ at the Ti/interlayer interface, and a two-phase (α-Ti + Ti_2Cu) region was observed on the Ti side. While clumpy $TiCu_4$ was formed in the melt interlayer, the liquid phase disappeared due to the extensive chemical reaction between Ti and Cu, leading to the formation of an Ag solid solution with fine Cu_2O precipitates. The bonding mechanisms could be categorized into various stages. In stage 1, melting and liquid phase separation were the predominant mechanisms. In stage 2, dissolution and reactive wetting were the predominant mechanisms. In stage 3, interdiffusion and/or chemical reactions between Ti and Cu were the predominant mechanisms. In stage 4, solidification was the predominant mechanism after Ti and Cu were consumed due to the formation of various Ti–Cu intermetallic compounds, increasing the liquidus of residual Ag–Cu above the brazing temperature. In the cooling stage, fine Cu_2O and/or Ti_3Cu_3O phases were precipitated in the residual interlayer, while a eutectoid reaction (α-Ti + Ti_2Cu) occurred on the Ti side for long-term brazing.

ACKNOWLEDGMENT

This research was supported by the National Science Council (Taiwan) under Contract No. NSC98-2221-E-009-039-MY2.

REFERENCES

1. O. Dezellus, J. Andrieux, F. Bosslet, M. Sacerdote-Peronnet, T. Baffie, F. Hodaj, N. Eustathopoulos, and J.C. Viala: Transient liquid phase bonding of titanium to aluminium nitride. *Mater. Sci. Eng., A* **495**, 254 (2008).
2. R.K. Shiue, S.K. Wu, F.Y. Chen, and T.E. Yang: Interfacial reactions and wettability of 72Ag-28Cu braze on CP-Ti substrate using infrared heating. *Metall. Mater. Trans. A* **43**, 1742 (2012).
3. C.C. Liu, C.L. Ou, and R.K. Shiue: The microstructural observation and wettability study of brazing Ti-6Al-4V and 304 stainless steel using three braze alloys. *J. Mater. Sci.* **37**(11), 2225 (2002).
4. D. Sotiropoulou and P. Nikolopoulos: Work of adhesion in ZrO_2 liquid-metal systems. *J. Mater. Sci.* **28**(2), 356 (1993).
5. W.D. Kingery, H.K. Bowen, and D.R. Uhlmann: *Introduction to Ceramics*, 2nd ed. (John Wiley & Sons, New York, 1991), p. 209.
6. A. Guedes, A.M.P. Pinto, M. Vieira, and F. Viana: Multulayered interface in Ti/Macor® machinable glass-ceramic joints. *Mater. Sci. Eng., A* **301**, 118 (2001).
7. W.B. Hanson, K.I. Ironside, and J.A. Fernie: Active metal brazing of zirconia. *Acta. Mater.* **48**(18–19), 4673 (2000).
8. H.Y. Chan, D.W. Liaw, and R.K. Shiue: The microstructural observation of brazing Ti-6Al-4V and TZM using the BAg-8 braze alloy. *Int. J. Refract. Met. Hard Mater.* **22**(1), 27 (2004).

https://doi.org/10.1557/jmr.2014.30 Published online by Cambridge University Press

9. Z.G. Wang, N. Kato, K. Sasaki, T. Hirayama, and H. Saka: Electron holographic mapping of two-dimensional doping areas in cross-sectional device specimens prepared by the lift-out technique based on a focused ion beam. *J. Electron Microsc.* **53**(2), 115 (2004).
10. G. Cliff and G.W. Lorimer: The quantitative analysis of thin specimens. *J. Microsc.* **103**(2), 203 (1975).
11. J.I. Goldstein, D.B. Williams, and G. Cliff: Quantitative x-ray analysis. In *Principles of Analytical Electron Microscopy*, D.C. Joy, A.D. Romig, and J.I. Goldstein eds.; Plenum Press: New York, 1986; p. 155.
12. J.L. Murray: Calculations of stable and metastable equilibrium diagrams of the Ag-Cu and Cd-Zn systems. *Metall. Trans. A* **15**(2), 261 (1984).
13. K.L. Lin, M. Singh, and R. Asthana: Interfacial characterization of YSZ-to-steel joints with Ag-Cu-Pd interlayers for solid oxide fuel cell applications. *Ceram. Int.* **38**(3), 1991 (2012).
14. G.W. Liu, W. Li, G.J. Qiao, H.J. Wang, J.F. Yang, and T.J. Lu: Microstructures and interfacial behavior of zirconia/stainless steel joint prepared by pressureless active brazing. *J. Alloys Compd.* **470** (1–2), 163 (2009).
15. Y.W. Chang and C.C. Lin: Compositional dependence of phase formation mechanisms at the interface between titanium and calcia-stabilized zirconia at 1550°C. *J. Am. Ceram. Soc.* **93**(11), 3893 (2010).
16. J.G. Lee, S.J. Hong, M.K. Lee, and C.K. Rhee: High strength bonding of titanium to stainless steel using an Ag interlayer. *J. Nucl. Mater.* **395**(1–3), 145 (2009).
17. J. Andrieux, O. Dezellus, F. Bosselet, M. Sacerdote-Peronnet, C. Sigala, R. Chiriac, and J.C. Viala: Details on the formation of Ti_2Cu_3 in the Ag-Cu-Ti system in the temperature range 790-860°C. *J. Phase Equilib. Diffus.* **29**(2), 156 (2008).
18. G.P. Kelkar, K.E. Spear, and A.H. Carim: Thermodynamic evaluation of reaction products and layering in brazed alumina joints. *J. Mater. Res.* **9**(9), 2244 (1994).
19. M.L. Santella, J.A. Horton, and J.J. Pak: Microstructure of alumina brazed with a silver-copper-titanium alloy. *J. Am. Ceram. Soc.* **73**(6), 1785 (1990).
20. H.J. Lee and H.I. Aaronson: Eutectoid decomposition mechanisms in hypoeutectoid Ti-X alloys. *J. Mater. Sci.* **23**(1), 150 (1988).
21. Y.H. Liang, H.Y. Wang, Y.F. Yang, Y.Y. Wang, and Q.C. Jiang: Evolution process of the synthesis of TiC in the Cu-Ti-C system. *J. Alloys Compd.* **452**(2), 298 (2008).
22. C. Hammerl, B. Renner, B. Rauschenbach, and W. Assmann: Phase formation in titanium after high-fluence oxygen ion implantation. *Nucl. Instrum. Methods Phys. Res., Sect. B* **148**(1–4), 851 (1999).
23. B. Holmberg: Disorder and order in solid solutions of oxygen in α-titanium. *Acta Chem. Scand.* **16**, 1245 (1962).
24. K.L. Lin and C.C. Lin: Reaction between titanium and zirconia powders during sintering at 1500°C. *J. Am. Ceram. Soc.* **90**(7), 2220 (2007).
25. J.S. Pimenta, A.J.A. Buschinelli, R.M. do Nascimento, A.E. Martinelli, and J. Remmel: Joining of zirconia mechanically metalized with titanium. *Cerâmica* **56**, 212 (2010).
26. A. Soon, M. Todorova, B. Delley, and C. Stampfl: Thermodynamic stability and structure of copper oxide surfaces: A first-principles investigation. *Phys. Rev. B* **75**, 125420 (2007).
27. V.N. Eremenko, Y.I. Buyanov, and N.M. Panchenko: Polythermal and isothermal sections of the system titanium-copper-silver. Part II. *Sov. Powder Metall. Met. Ceram.* **9**(5), 410 (1970).
28. V.N. Eremenko, Y.I. Buyanov, and N.M. Panchenko: The liquidus surface of the system titanium-copper-silver. *Powder Metall. Met. Ceram.* **9**(4), 301 (1970).
29. J.L. Murray and K.J. Bhansali: The Ag-Ti (silver-titanium) system. *J. Phase Equil.* **4**(2), 178 (1983).
30. J.L. Murray: The Cu-Ti (copper-titanium) system. *J. Phase Equil.* **4**(1), 81 (1983).
31. S. Hirnyj and J.E. Indacochea: Phase transformations in Ag70.5Cu26.5Ti3 filler alloy during brazing processes. *Chem. Met. Alloys* **1**, 323 (2008).
32. M. Yang, T. Lin, and P. He: Microstructure evolution of Al_2O_3/Al_2O_3 joint brazed with Ag-Cu-Ti + B + TiH_2 composite filler. *Ceram. Int.* **38**, 289 (2012).
33. R.H. Shiue and S.K. Wu: Infrared brazing $Ti_{50}Ni_{50}$ and Ti-6Al-4V using the BAg-8 braze alloy. *Mater. Trans.* **46**(9), 2057 (2005).

https://doi.org/10.1557/jmr.2014.30 Published online by Cambridge University Press